FAST FOURIER TRANSFORM ANALYSIS OF ROTOR-BEARING SYSTEMS

K. C. Choy, Post Doctoral Fellow
E. J. Gunter, Professor
Department of Mechanical and Aerospace Engineering
School of Engineering and Applied Science
University of Virginia
Charlottesville, Virginia

ABSTRACT

Nonlinear transient analysis of rotor-bearing systems is becoming increasingly important in the analysis of modern-day rotating machinery to model such phenomena as oil film whirl. This paper develops an analysis technique incorporating modal analysis and fast Fourier transform techniques to analyze rotors with residual shaft bow and realistic nonlinear bearings. The technique is demonstrated on single-mass and three-mass rotor examples. Comparisons of the theoretical results with experimental data give excellent agreement.

NOMENCLATURE

Symbol	Description
$[A]$	Orthonormal mode matrix = $\begin{bmatrix} A_e \\ \hline A_\beta \end{bmatrix}$
$[A_e]$	Translation orthonormal mode matrix
$[A_\beta]$	Rotational orthonormal mode matrix
C	Bearing clearance
C_{ij}	Modal damping coefficients
$C_{xx}, C_{xy}, C_{yx}, C_{yy}$	Bearing damping coefficients
$[C]$	Damping matrix
$[C_b]$	Bearing damping matrix
$F_b(x, y, \dot{x}, \dot{y})$	Nonlinear bearing forces
F_x, F_y	External applied forcing functions
f_r	Radial nonlinear bearing force
f_t	Tangential nonlinear bearing force
h	Bearing film thickness

I_{ti}	Transverse moment of inertia at ith station
I_{pi}	Polar moment of inertia at ith station
$[I_t]$	Moment of inertia matrix
K_b	Average principle bearing stiffness, $(K_{xx} + K_{yy})/2$
$K_{xx}, K_{xy}, K_{yx}, K_{yy}$	Bearing Stiffness
$K_{x\theta}$, $K_{x\psi}$, etc.	Bearing axial misalignment stiffness (generally small)
$k_{xx}, k_{x\theta}, k_{\theta x}, k_{\theta\theta}$	Shaft stiffness
$[K]$	Total system stiffness matrix
$[K_B]$	Bearing stiffness matrix
$[K_s]$	Shaft stiffness matrix
L	Section length
M	Mass of journal acting at bearing
$[M]$	Mass matrix
N_c	Critical speed
$\bar{P}$	Pressure in bearing
R	Shaft radius
Q	Aerodynamic cross-coupling coefficient
$q_i(t)$	Modal constant of ith undamped mode
U_i	Modal unbalance of ith mode
U_d	Unbalance weight
$\{U\}$	Displacement vector of system
W	Weight of journal
x_i, y_i	Total displacement at ith mass station
x_{di}, y_{di}	Shaft mechanical bow at ith mass station
z	Axial coordinate
ϵ	Eccentricity ratio of journal, e/C
μ	Viscosity of fluid lubricant
σ	Modified Sommerfeld number
ω_i	The ith undamped critical speed of the system
θ	Shaft transverse angle in x direction
ψ	Shaft transverse angle in y direction
$\bar{\phi}$	Precession angle of shaft
Ω	Angle around bearing

INTRODUCTION

Generally, the modern-day analyses of rotor-bearing system are conveniently divided into critical speed and stability analysis (1, 2), unbalance response (3, 4), balancing (5, 6), and transient response (7 - 18). All categories except the last are linearized approximations to the real system. In many cases, such as with realistic fluid film bearings undergoing oil whirl, only nonlinear transient analysis is capable of modeling the rotating machine accurately (17).

The objective of this paper is to develop an analysis technique incorporating features which contribute to the understanding of the real

system (18, 19). Modal analysis is employed for rapid, low-cost integration in time but easy to obtain planar modes with average bearing stiffnesses give designers an approximate indication of rotor mode shapes. Residual bow (4, 5) and realistic bearing forces (20-22) are included. A fast Fourier transform technique (23, 24) enables conventional rotor orbits, which are shown in many rotor dynamics papers, to be easily interpreted for frequency content. While this technique has been employed in earthquake structural analysis, there does not appear to be any discussion in the rotor dynamics literature.

A comparison of the analysis with experimental data is carried out for a three-mass bowed rotor in plain journal bearing (20). The rotor undergoes oil whirl (or oil whip, as some authors prefer) at high speed. With the inclusion of nonlinear bearing forces in the rotor model, good agreement was obtained between theory and experimental results.

FORCED RESPONSE ANALYSIS USING MODAL ANALYSIS

This work employs a modal analysis for rotor systems using uncoupled undamped mode shapes including average bearing (or seal) linearized stiffness properties. These mode shapes are relatively easy to obtain (computer codes to accomplish this are widely available in industry) and are planar in form. Much more physical "feel" for the rotor motion is possible than with free-free modes, but the coupling terms must not be neglected in the full system analysis. The planar modes are then used to obtain damped natural frequencies and forced response.

Details of the derivation are given in references (12, 13, 18, 19) and are omitted here at the suggestion of the reviewers. A verbal outline is given instead.

In solving for the forced response of the rotor-bearing system, the matrix equation of motion in Appendix A is transformed into modal coordinates using a set of undamped orthogonal planar modes. With the effects of unbalance, disc skew, shaft bow, and rotor acceleration, the set of modal equations in the x-z plane can be written as follows:

$$\begin{bmatrix} [M] & 0 \\ 0 & [I_t] \end{bmatrix} \begin{bmatrix} [A_e] \\ [A_\beta] \end{bmatrix} \begin{bmatrix} \ddot{q}_x \end{bmatrix} + \begin{bmatrix} [C_{xx}] & [C_{x\theta}] \\ [C_{\theta x}] & [C_{\theta\theta}] \end{bmatrix} \begin{bmatrix} [A_e] \\ [A_\beta] \end{bmatrix} \begin{bmatrix} \dot{q}_x \end{bmatrix}$$

$$+ \begin{bmatrix} [k_{xx}+K_b] & [k_{x\theta}] \\ [k_{\theta x}] & [k_{\theta\theta}] \end{bmatrix} \begin{bmatrix} [A_e] \\ [A_\beta] \end{bmatrix} \begin{bmatrix} q_x \end{bmatrix} - \begin{bmatrix} [k_{xx}] & [k_{x\theta}] \\ [k_{\theta x}] & [k_{\theta\theta}] \end{bmatrix} \begin{bmatrix} [X_d] \\ [\theta_d] \end{bmatrix}$$

$$+ \begin{bmatrix} [K_{xx}-K_b] & [K_{x\theta}] \\ [K_{\theta x}] & [K_{\theta\theta}] \end{bmatrix} \begin{bmatrix} [A_e] \\ [A_\beta] \end{bmatrix} \begin{bmatrix} q_x \end{bmatrix} + \begin{bmatrix} [C_{xy}] & [C_{x\psi}] \\ [C_{\theta y}] & [C_{\theta\psi}] \end{bmatrix} \begin{bmatrix} [A_e] \\ [A_\beta] \end{bmatrix} \begin{bmatrix} \dot{q}_y \end{bmatrix}$$

$$+\begin{bmatrix} 0 & 0 \\ 0 & [\omega I_p] \end{bmatrix}\begin{bmatrix} [A_e] \\ [A_\beta] \end{bmatrix}\begin{Bmatrix} \dot{q}_y \end{Bmatrix}+\begin{bmatrix} [K_{xy}] & [K_{x\psi}] \\ [K_{\theta y}] & [K_{\theta\psi}] \end{bmatrix}\begin{bmatrix} [A_e] \\ [A_\beta] \end{bmatrix}\begin{Bmatrix} q_y \end{Bmatrix}$$

$$+\begin{bmatrix} 0 & 0 \\ 0 & [\tfrac{1}{2}\dot{\omega} I_p] \end{bmatrix}\begin{bmatrix} [A_e] \\ [A_\beta] \end{bmatrix}\begin{Bmatrix} q_y \end{Bmatrix}=\begin{Bmatrix} F(t) \end{Bmatrix} \qquad (1)$$

Note that all the terms in the left-hand side of the equation are represented by generalized coordinates (q_x, q_y) except for the bow of the shaft. In the modal approach as discussed in (18, 19), it was noted that for general cases the shaft stiffness matrix of the shaft is not required after the modal transformation while equation (1) has to retain the stiffness matrix in order to include the shaft bow effects. To avoid the derivation of the stiffness matrix and to save computer time and core memory space, the bow of the shaft is transformed into modal coordinates.

After resolving the shaft bow terms into modal coordinates, equation (1) is premultiplied by the transpose of the translation and rotational orthonormal mode matrices [A]. All terms not containing mode shapes q_x and q_y are transferred to the right-hand side to form the equations of motion in modal form. The equations in the x-z plane are then added to the equivalent modal equations in the y-z plane. Solving for the modal acceleration terms yields an initial value problem. After initial modal displacements and velocity terms are specified, the modal transient motion is obtained by numerical integration in time. Rotor forced response is then obtained by back substitution into the equation:

$$\begin{Bmatrix} U(t) \end{Bmatrix}=\begin{Bmatrix} x(t) \\ \theta(t) \\ y(t) \\ \psi(t) \end{Bmatrix}=\begin{Bmatrix} \begin{bmatrix} [A_e] \\ [A_\beta] \end{bmatrix}\begin{Bmatrix} q_x(t) \end{Bmatrix} \\ \begin{bmatrix} [A_e] \\ [A_\beta] \end{bmatrix}\begin{Bmatrix} q_y(t) \end{Bmatrix} \end{Bmatrix} \qquad (2)$$

The planar undamped modes as well as free-free modes have been used by Childs previously (12, 13), but the equations including disc skew and shaft bow have not been shown in the literature. In the experimental three-mass rotor presented later, the shaft residual bow was found to be of approximately the same size as the deflection due to unbalance near the critical speed even for a well-balanced rotor. The comparison between theory and experiment will show the effects of the residual bow. Disk skew effects in the experimental rotor were small, but the terms in the equations of motion are included here for completeness.

No demonstration of the accuracy and rapidity of this modal method will be given here due to length considerations. An extensive comparison of the method to the transfer matrix method and modal methods employing free-free modes is given in (18, 19). The comparisons were carried out

for the linearized stability of a compressor whose geometry is given in the literature (2). Results indicated that the planar undamped modal analysis using averaged bearing stiffness is an efficient calculation method for rotors with hydrodynamic bearings. As the results are not for nonlinear transient work and the advantages of modal analysis are well known, they are omitted here.

NONLINEAR MODAL TRANSIENT ANALYSIS

In transient analysis of many mechanical structures, the accelerations obtained by solving the equations of motion are integrated directly to evaluate the dynamic transient response of the system. In this particular analysis, the modal equations of motion with modal excitations are solved, and the modal accelerations are integrated directly by numerical integration. The stability and accuracy of different types of numerical integration procedures have been extensively discussed. These considerations are beyond the scope of this research. In this study, the main concern is the application of a simple, accurate numerical integration scheme in nonlinear transient response analysis of turbomachinery, especially when a large number of integration steps are necessary. For direct integration of the equations of motion using the point mass stiffness formulation, the modal acceleration equation can be rewritten in the following form.

$$\{\ddot{U}\} = \begin{Bmatrix} (\ddot{x}) \\ (\ddot{\theta}) \\ (\ddot{y}) \\ (\ddot{\psi}) \end{Bmatrix} = -[M^{-1}] \left\{ [C]\{\dot{U}\} + [K]\{U\} - \{F(t)\} \right\} \qquad (3)$$

With this equation, the acceleration quantities {U} may be calculated starting from the initial conditions. Using the summation notation convention, the coupled equations may be written as

$$\ddot{u}_i = -\bar{C}_{ij}\dot{u}_j - \bar{K}_{ij}u_j + F_i(t, \dot{u}_i, u_i) \qquad (4)$$

where $\bar{C} = M^{-1} C$, $\bar{K} = M^{-1} K$

There are numerious procedures that have been proposed for numerical integration of this type of equation, but the Newmark Beta method has been found successful here.

In modal analysis, the bearing forces of the system are incorporated into modal equations of motion as modal forces F_{bx} and F_{by} (Appendix B). These modal forces are combined together with other excitations, such as rotor unbalance, disk skew, and shaft bow, to form the total modal excitation of the system. The modal bearing forces can be calculated by

$$\{F_{bx}\} = [A_e]^T \{F_x\} \qquad (5)$$

$$\{F_{by}\} = [A_e]^T \{F_y\} \qquad (6)$$

where F_x and F_y are the bearing force vectors at the mass stations.

In this particular analysis, the effects of nonlinear bearing forces can be illustrated using short journal bearings (21, 22) whose bearing forces can be represented by an analytical expression. Values for F_x and F_y are obtained in Appendix B. Previous work (17) employing a full finite difference solution to Reynolds equation has been quite expensive in terms of computer costs.

FREQUENCY ANALYSIS OF TRANSIENT RESPONSE USING DISCRETE FAST FOURIER TRANSFORMATION

In the analysis of transient response of rotor-bearing systems, it may sometimes be difficult to interpret results from transient response orbits or from time-displacement plots, especially for a complex rotor system. The use of the Fourier transformation simulating a "spectrum analyzer" numerically by digital computer is likely to be a powerful technique in transient response analysis. It also provides information concerning the nonlinear stability of the system.

In applying the Fourier transformation, the response of the system in the time domain is transformed into the frequency domain as

$$\bar{F}\ (i\omega) = \int_{-\infty}^{\infty} f(t)\ e^{i\omega t}\ dt \tag{7}$$

$$\bar{F}_m\ (i\omega) = \sum_{n=0}^{N-1} f_n\ e^{-i(2\pi m\ n/N)}\ ,\ m = 0,\ 1,\ 2,\ \ldots,\ N-1 \tag{8}$$

where m = frequency index
N = total number of samples
f_n = n^{th} sample of f(t)

Using the above equations, the transient response of the system is transformed into discrete frequency responses which are the "densities" or "excitations" of the corresponding frequencies. In other words, the response after the transformation are the magnitudes at which these frequencies will be excited.

A more efficient algorithm is the fast Fourier transformation (23, 24) by which the repetitions in the discrete Fourier transformation calculations are eliminated. With N as a multiple of P, the frequency responses of the system are given by

$$\bar{F}_m = \bar{A}_m + W_N^{\ m}\ \bar{B}_m,\ m = 0,\ 1,\ 2,\ \ldots\ P-1 \tag{9}$$

where

$$\bar{A}_m = \sum_{n=0}^{P-1} f_{2n}\ W_p^{\ mn}$$

$$\bar{B}_m = \sum_{n=0}^{P-1} f_{2n+1}\ W_p^{\ mn}$$

$$W_p = e^{-i\left(\frac{2\pi}{P}\right)} = \left(e^{-i\left(\frac{2\pi}{N}\right)}\right)^2$$

$$W_N = \sqrt{W_p}$$

Since the Fourier transformation is applied to periodic functions, it is necessary to use the whole series of real time transient motion as sample input for one sample period. Also, in order to avoid overlapping of the periodic motions, a series of zeros may be attached at the rear part of the sample input such that each period is separated and will not affect each other.

To illustrate the use of the Fourier transformation in transient bearing analysis, a single mass rotor on flexible bearings with internal damping effects similar to the one analyzed by Gunter (1) was examined.

$M = 0.25$ lb-sec^2/in	K (shaft) = 250,000 lb/in
K = 125,000 lb/in	K = 250,000 lb/in
C_1 (bearing) = 50 lb-sec/in	C_2 (internal) = 50 lb-sec/in

The rotor is run through a series of constant shaft speeds ranging from 10,000 RPM to 30,000 RPM. The shaft is released from a position in space and undergoes a transient motion until it settles down into a limit cycle. Figures 1, 2, 3, and 4 show the transient response of the rotor with various operating speeds. When the rotor is operating under 30,000 RPM, it can be seen from the figure that the transient response of the system decays with time until it settles into steady-state motion with a small orbit. When the rotor is running at 30,000 RPM, the orbit size does not decrease with time and is almost constant. This means that the rotor is operating near its stability threshold speed. The inside loop in the transient response indicates the existence of large nonsynchronous components. When the operating speed is raised, for example to 35,000 RPM as shown in Fig. 4, it can be seen that the rotor system is unstable. The transient response is increasing with time and the response orbit is growing out to some large limit cycle.

Using the Fourier transformation, as discussed previously, the rotor transient response can be transformed into frequency components and can be expressed in a frequency spectrum or "waterfall" diagram, as shown in Fig. 5. From this frequency spectrum, one can visualize more easily the stability, component response, and resonance speeds of the system.

The decrease in magnitudes of the synchronous component and increase in magnitude of the nonsynchronous components with speed indicates that the stability decreases with the increase of speed. The large non-synchronous components with speed indicates that the stability decreases with the increase of speed. The large nonsynchronous component at 30,000 RPM occurs near 7,000 RPM, which is at a multiple of one of the critical speeds of the system, shows the instability excited by the first critical speed frequency (N_{c_1} = 6,751 RPM or 707 rad/sec).

The above example demonstrates the use of Fourier transformation in frequency analysis of rotor transient motion when nonlinear bearings or other nonlinear forces exist in the system while linear stability analysis of the system fails. The method reduces a large number of orbital plots, often difficult to interpret, to a single graph indicating the spectral components through the rotor speed range.

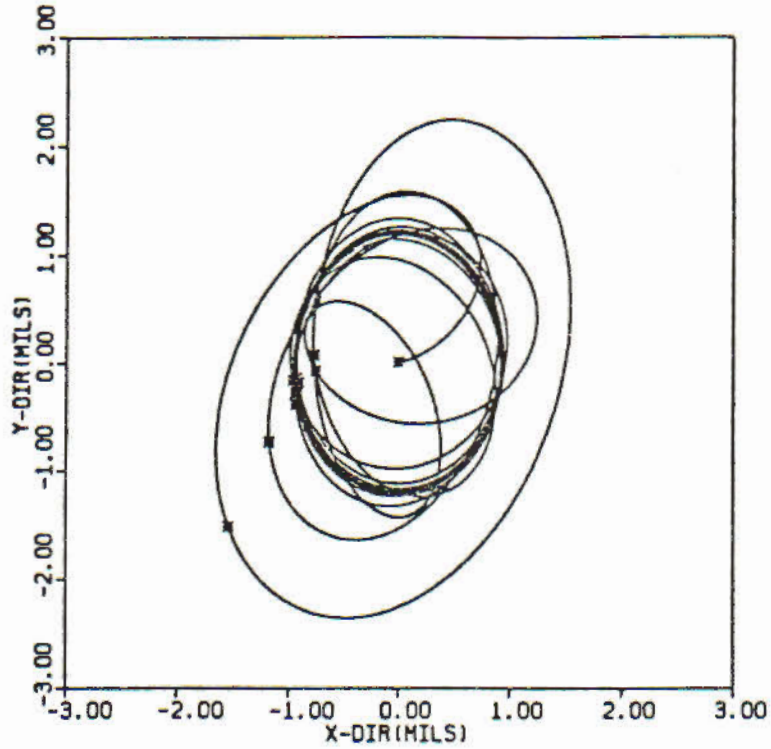

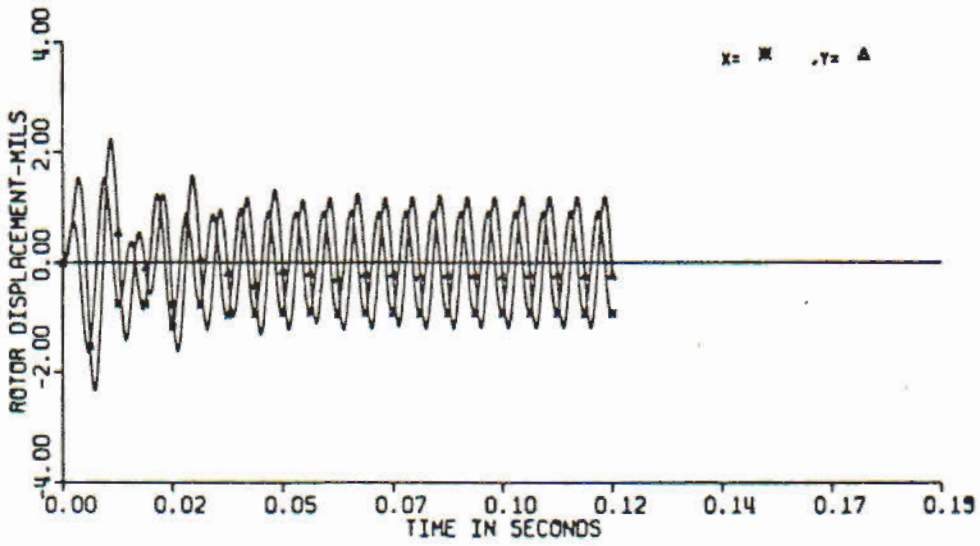

Fig. 1 Transient Motion of Single Mass Rotor at 10,000 RPM

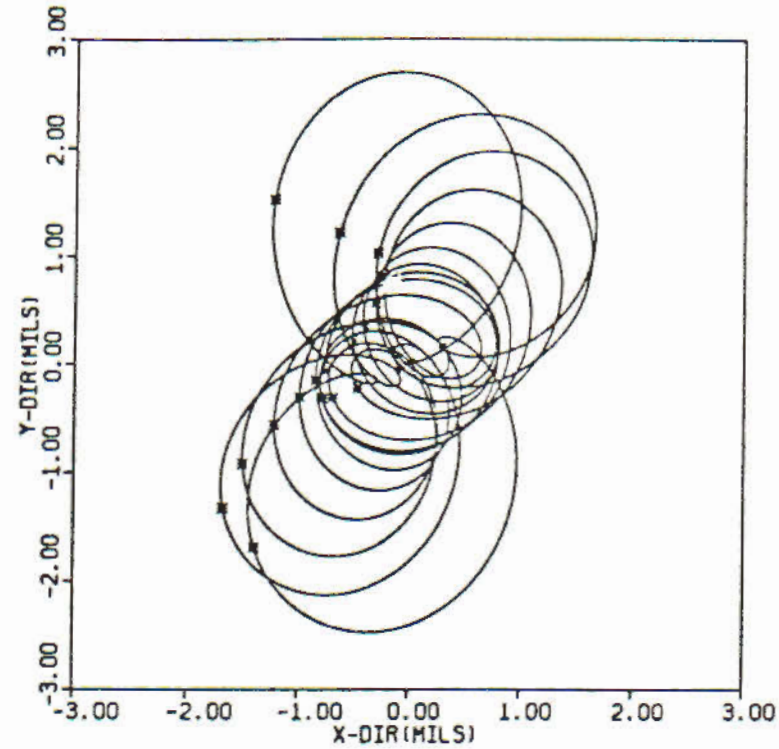

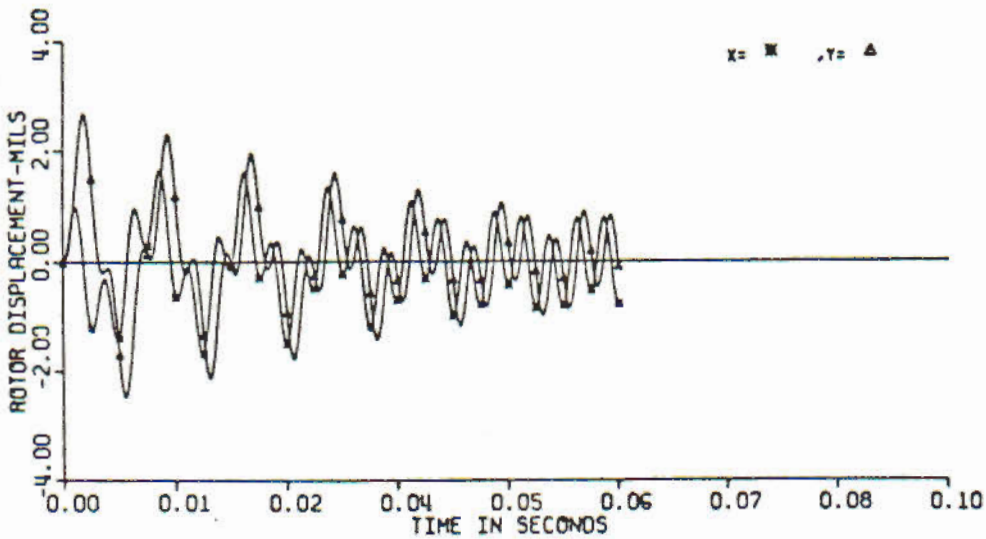

Fig. 2 Transient Motion of Single Mass Rotor at 20,000 RPM

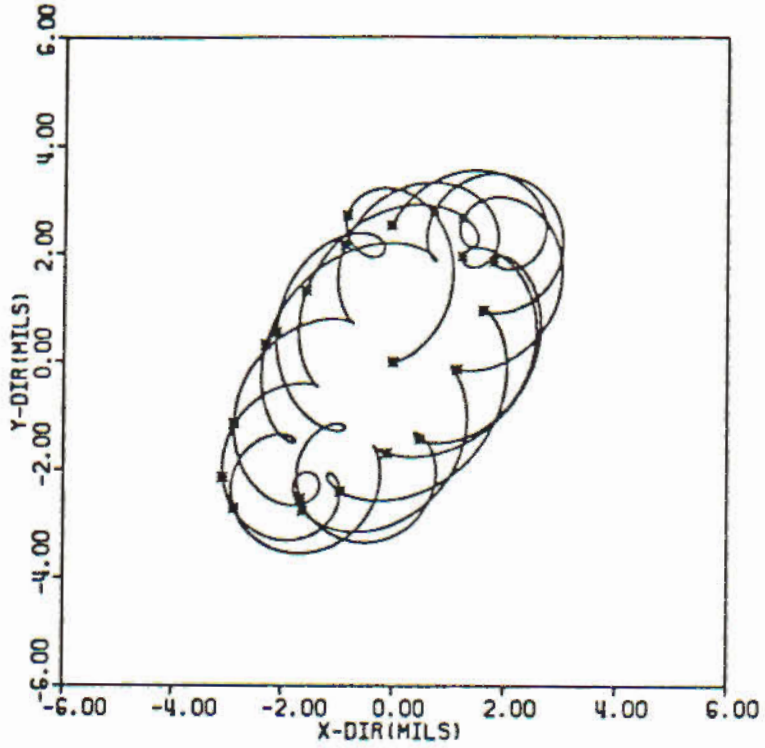

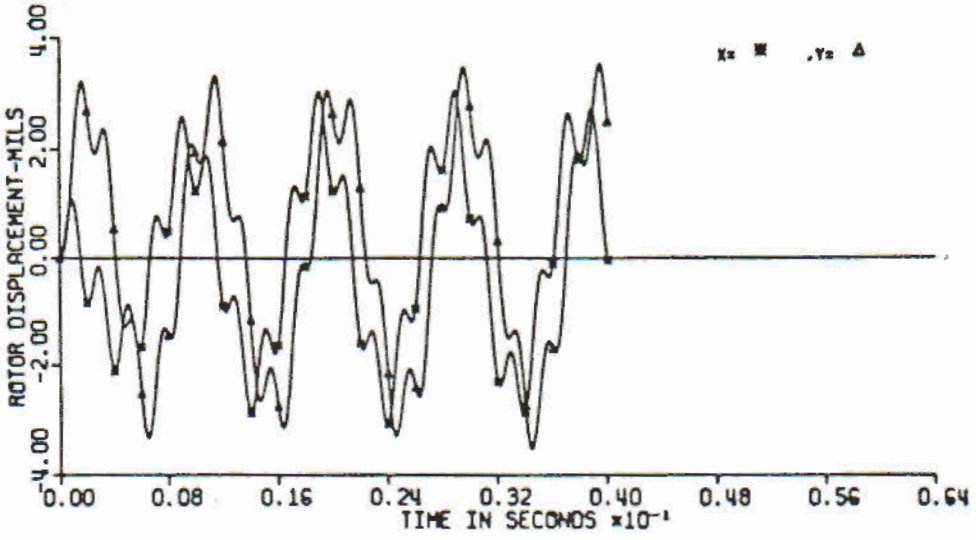

Fig. 3 Transient Motion of Single Mass Rotor at 30,000 RPM

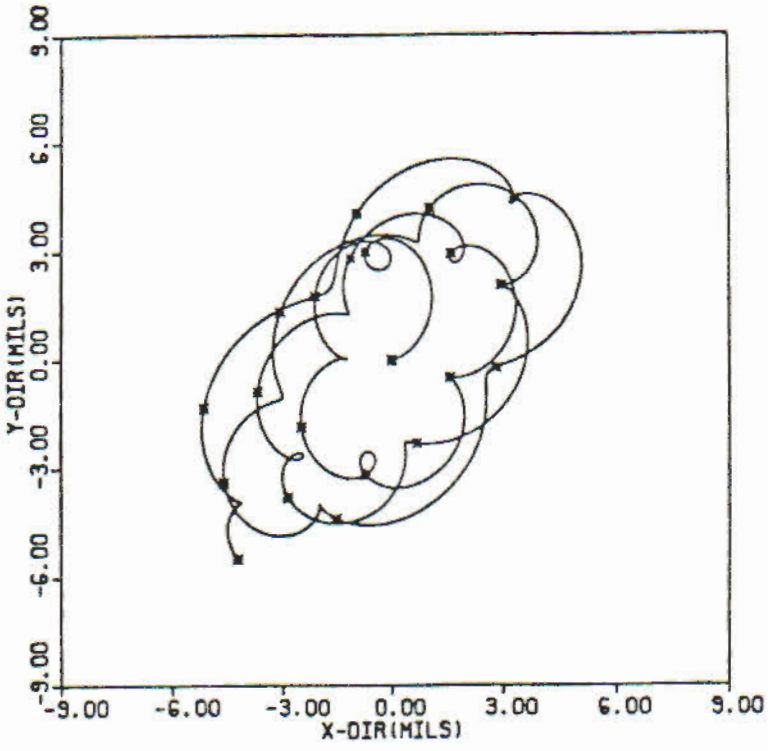

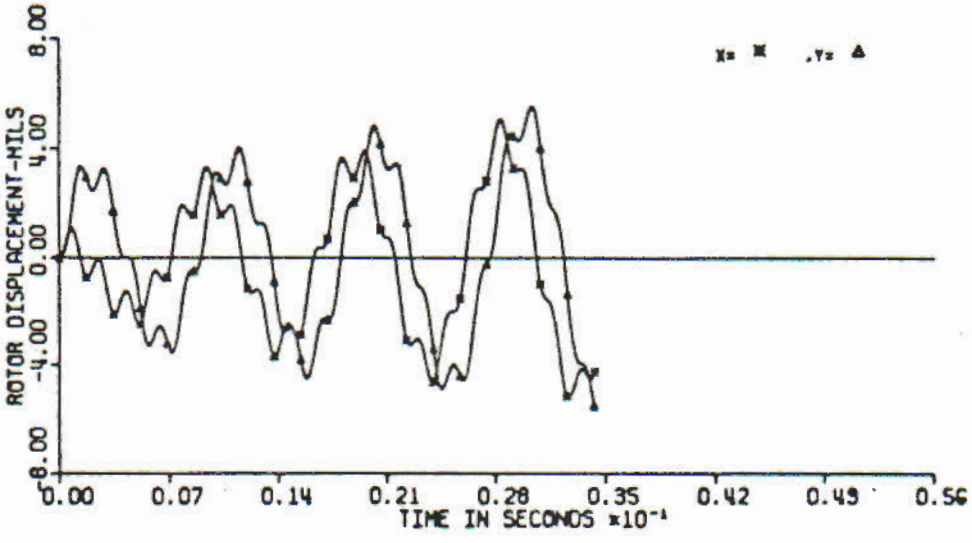

Fig. 4 Transient Motion of Single Mass Rotor at 35,000 RPM

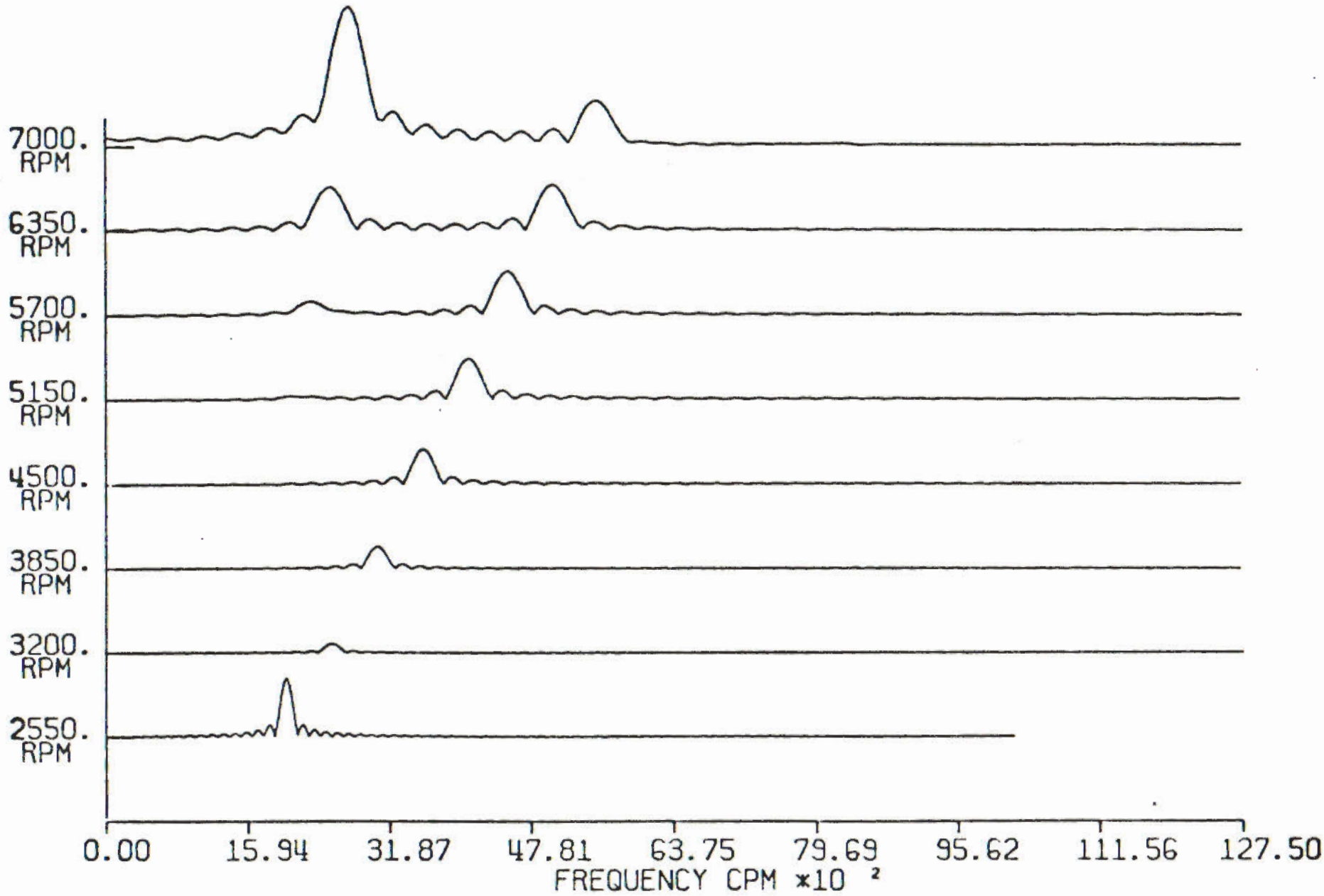

Fig. 5 Frequency Spectrum for the Single Mass Rotor

CORRELATION OF EXPERIMENTAL DATA WITH ANALYSIS

To illustrate the calculation of nonlinear forced response for a complex rotor, the results from the modal method were compared to experimental data. A uniform rotor of 21 in. long, 1 in. diameter with 3 large 9-lb. disks located at or near the mid span was used as the model for analysis. The rotor is supported by two plain journal bearings at each end. A schematic of the rotor system is given in Fig. 6. A non-contacting probe is set up in the position x2 as in the diagram monitoring the horizontal rotor motion near the mass.

The solid lines in Fig. 7 indicate the rotor synchronous response from experimental data (20). The dotted line represents the steady-state unbalance response calculation using only the first undamped planar mode of the system with averaged bearing stiffness. In this particular case, the unbalance of the system is measured to be 0.2 oz-in at 0 degrees located at the center dial of the rotor. The rotor has a residual bow of 0.7 mils at the center disk and 0.6 mils at the other disks. The bow vectors are 175 degrees out of phase with the rotor unbalance. The dotted line of modal calculations in Fig. 7 shows very good agreement with the experimental results. Note that there are differences in response during up and down speed of the rotor while the unbalance response calculation predicts an approximate average between them. Also, there occurs a dip in the response after the resonance peak, which indicates a residual bow in the rotor (4). It can also be seen that the dip in the rotor response did not go to zero, which indicates that the bow and the unbalance are less than 180 degrees out of phase with each other.

Using linear bearing stiffness, the rotor has a first undamped critical speed near 3,000 RPM. Since all the masses are lumped near the center of the rotor, the second critical speed of the rotor is very high compared to the first critical (over 20,000 RPM). Figure 8 shows the experimental frequency spectrum (waterfall) diagram of the system at various steady-state operating speeds. It can be seen that the critical speed of the system comes in near 2,500 RPM, and the dip of the response due to the mechanical bow of the system occurs at 3,200 RPM. Figure 6 shows both the synchronous and transient response of the rotor at various speeds (17).

It is also noted that the subsynchronous component becomes significant beyond 6,000 RPM, which is near the stability threshold speed of the system. The instability of the system is due to the half frequency whirl motion of the supporting journal bearings.

In using modal analysis, the rotor was modelled with 17 mass stations. Since the second critical speed is much higher than the first and is far beyond the operating speed range, only the first critical speed mode is used in this analysis. Transient responses of the system are calculated with nonlinear journal bearing forces (as discussed in the previous sections). Figure 9 shows the transient motion of the rotor center mass near the first critical speed at 2,550 RPM. The rotor is stable at this operating speed and the transient response of the system goes into steady-state motion. Figure 10 shows the transient motion of the rotor near the stability threshold speed (6,350 RPM). The occurence of an inside loop in the transient response orbit indicates the half-frequency whirl motion of the system. Figure 11 shows the transient motion of the system beyond the stability threshold speed (at 7,000 RPM). The rotor response is growing and does not settle into steady-state motion for the number of cycles calculated. Note that the existence of the inside loop type of transient orbit at the beginning gradually becomes a 2 to 1 whirl ratio motion. For a purpose of further understanding, the transient response was simulated for another 160 cycles of transient motion.

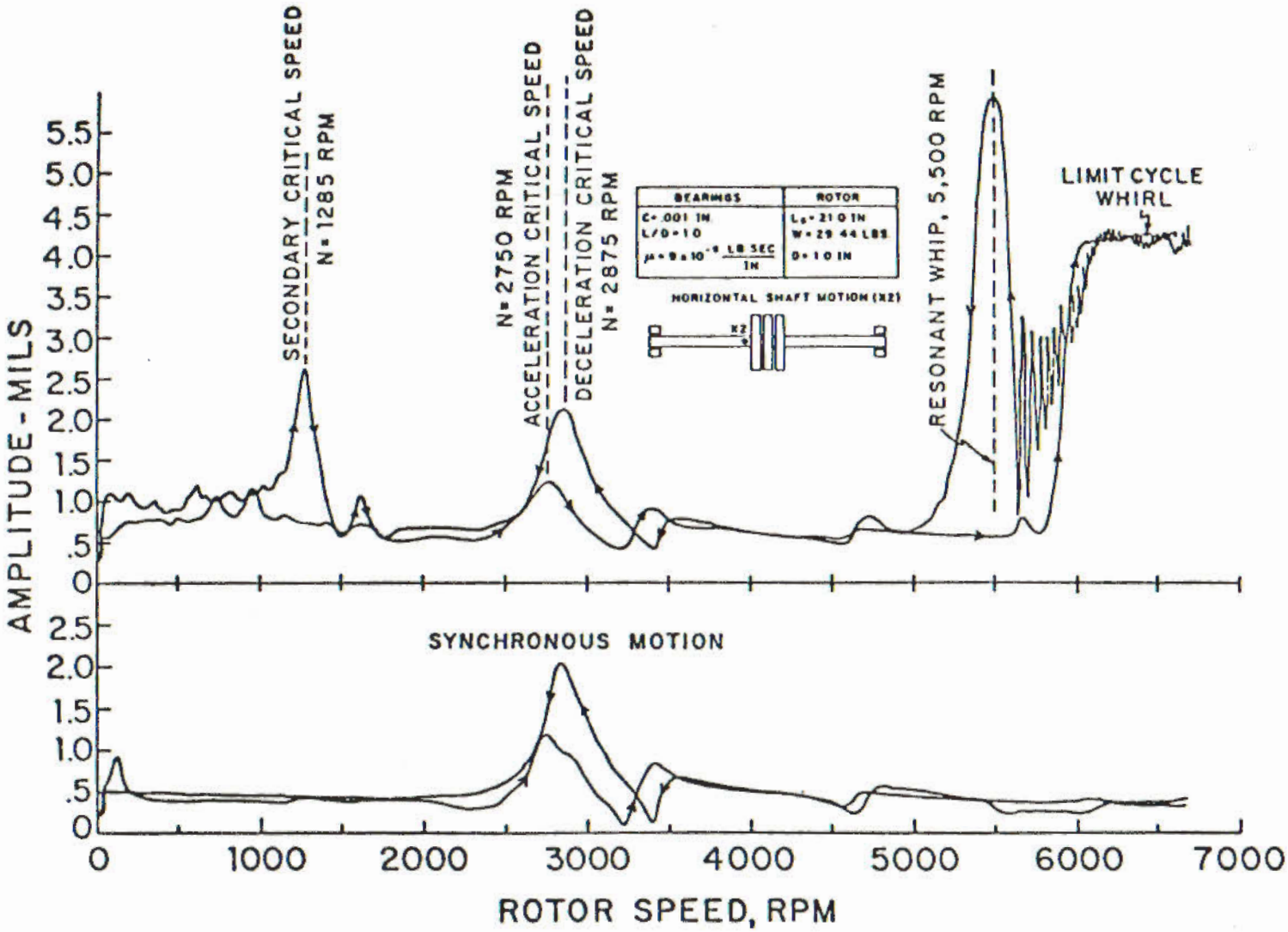

Fig. 6 Experimental Results of 3-Mass Rotor with Nonlinear Fluid Film Bearings

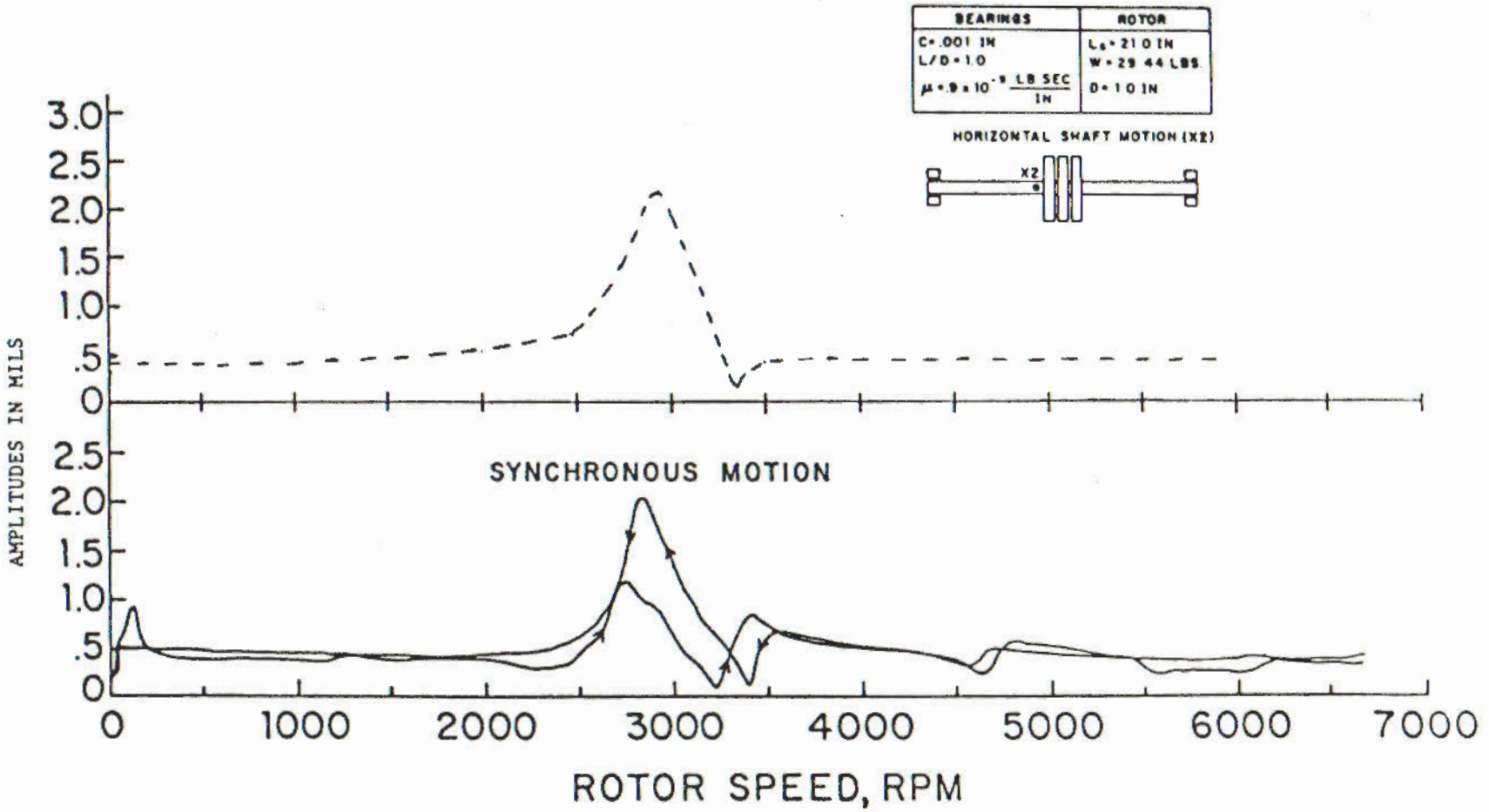

Fig. 7 Comparison of Theoretical and Experimental Results for 3-Mass Rotor

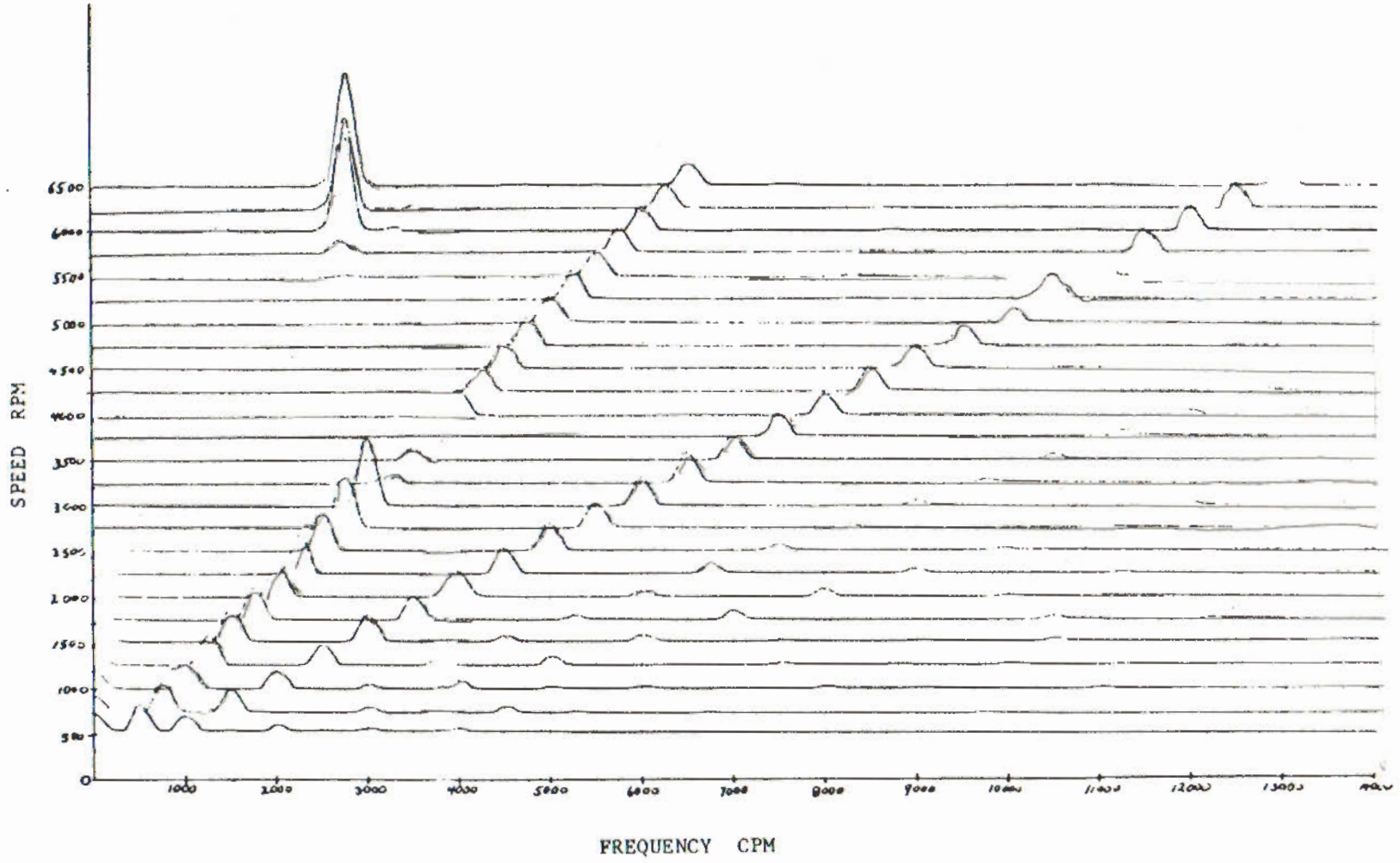

Fig. 8 Experimental Frequency Spectrum of 3-Mass Rotor with Fluid Film Bearings

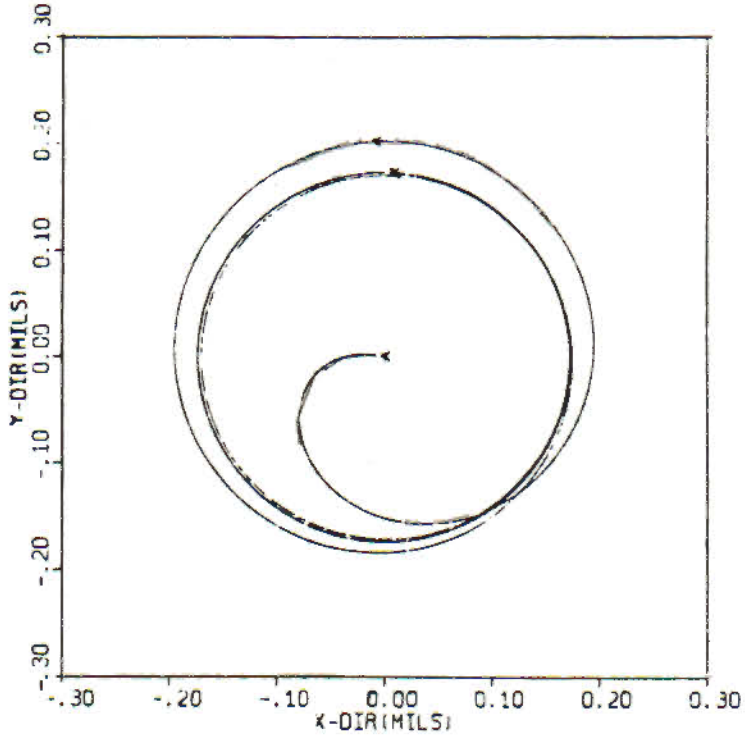

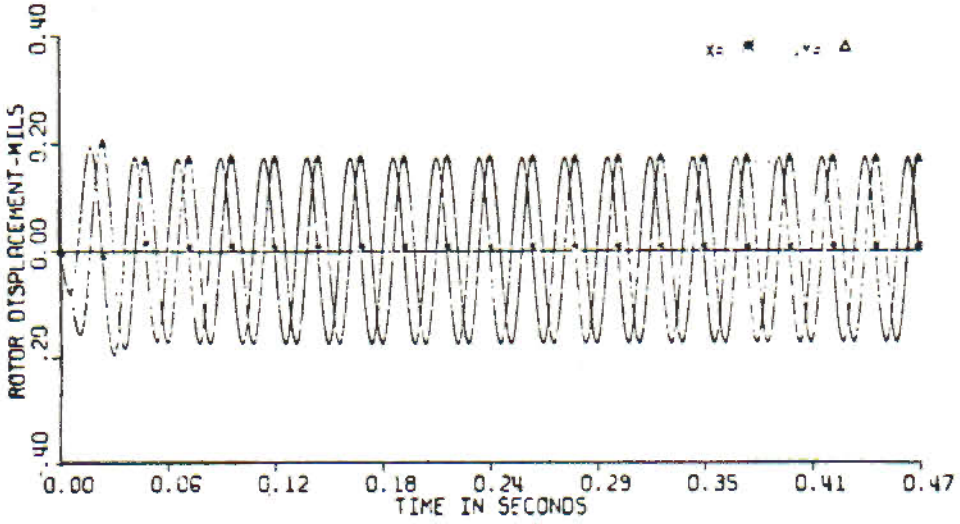

Fig. 9 Transient Simulation of 3-Mass Rotor with Fluid Film Bearings at 2,550 RPM

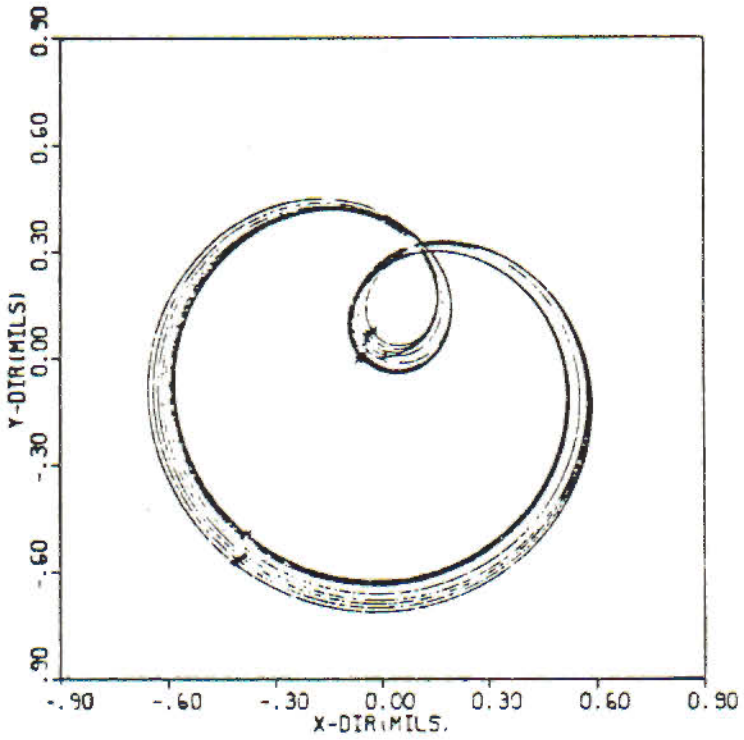

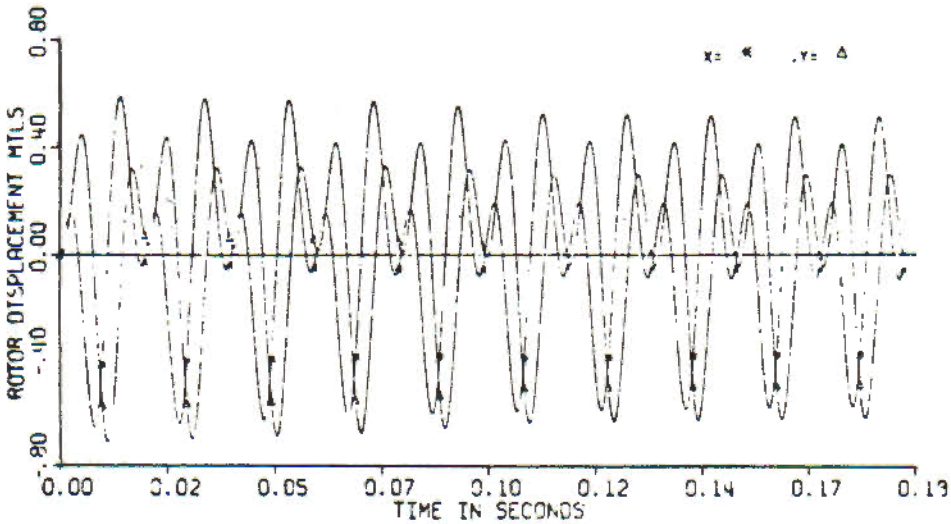

Fig. 10 Transient Simulation of 3-Mass Rotor with Fluid Film Bearings at 6,350 RPM

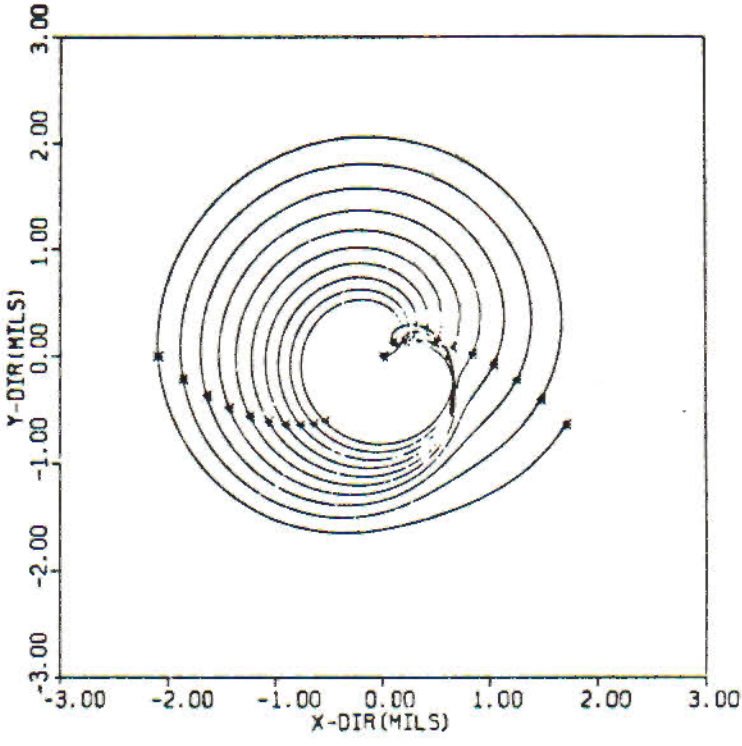

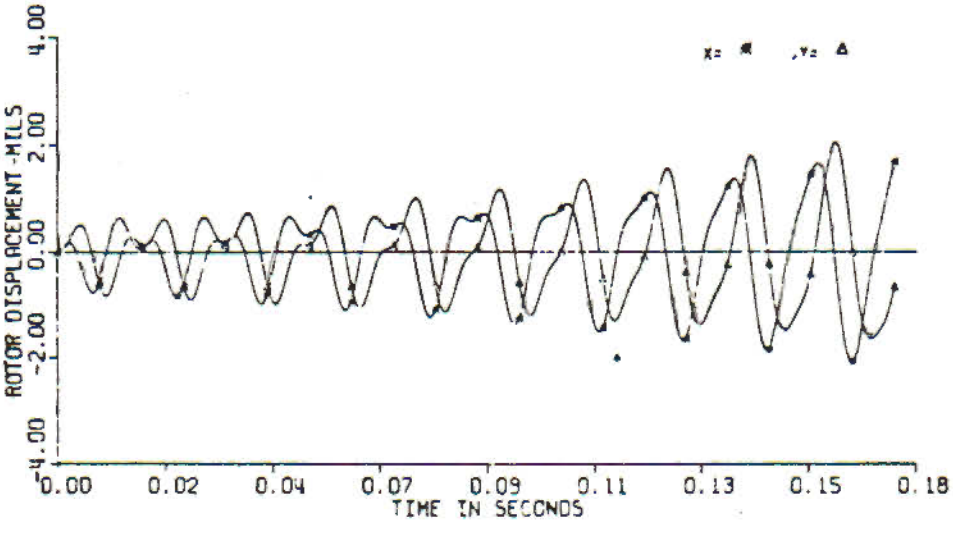

Fig. 11 Transient Simulation of 3-Mass Rotor with Fluid Film Bearings at 7,000 RPM

Figure 12 shows the transient motion of the center mass after 160 cycles where the transient orbit is settling into limit cycle. This phenomenon can only be predicted with the inclusion of nonlinear bearing forces. With the presence of this limit cycle, the stability of the system may sometimes be very difficult to interpret from transient orbits and a frequency analysis of the transient response is very useful.

The fast Fourier transformation discussed in the previous section is applied to the calculated transient motion. A frequency spectrum using the results of the transformation is given in Fig. 13. Note that the diagram is very similar to the experimental data (critical speed occurs near 2,550 RPM). The lack of higher nonsynchronous components (2 or 3 times running speed components) in this frequency spectrum as compared to the experimental data is due to electrical runout, coupling misalignment, and shaft asymmetry. From the above investigation, it can be concluded that the modal approach discussed in this study can be a fast and powerful technique in predicting dynamic behavior of rotor-bearing systems.

CONCLUSIONS

1. Modal equations of motion using planar undamped mode shapes have been developed in other works for the forced response of rotor-bearing systems. These equations include the effects of unbalance, disk skew, shaft bow, and rotor acceleration. The modal analysis is employed to produce a nonlinear transient response of the rotor including nonlinear bearing forces.

2. A numerical discrete fast Fourier transform technique has been introduced as a method for interpretation of rotor orbits. These provide the designer of rotor-bearing systems with relatively easy to interpret results in terms of frequency and amplitude content, and it also enables many orbits to be reduced into a single plot conveying much information.

3. Transient analysis of a single mass rotor at constant shaft speed with nonlinear bearing forces has been compared to previous work for verification purposes and demonstration of the numerical fast Fourier transform.

4. A nonlinear transient analysis at constant shaft speed has been carried out for a three-mass rotor with plain journal bearings and shaft bow. The results are compared to experimental measurements of the rotor. Prediction of the system critical speed, dip in synchronous response due to shaft bow, instability onset speed, and nonlinear sub-synchronous motion in oil whirl are excellent.

5. The examples used in this paper have been limited to simple rotor-bearing systems. The application of this work on more complicated systems with a large number of modes has also been successful and will be discussed in a later paper.

ACKNOWLEDGEMENT

This research was supported by Bearing Division, W. J. Anderson, Director, NASA Lewis Research Center, under Dr. David Fleming, Fluid Film Bearing Section Chief, and Robert Cunningham, Project Director. The authors would like to express their appreciation for the assistance and support received from Dr. Fleming and Mr. Cunningham for development of this work.

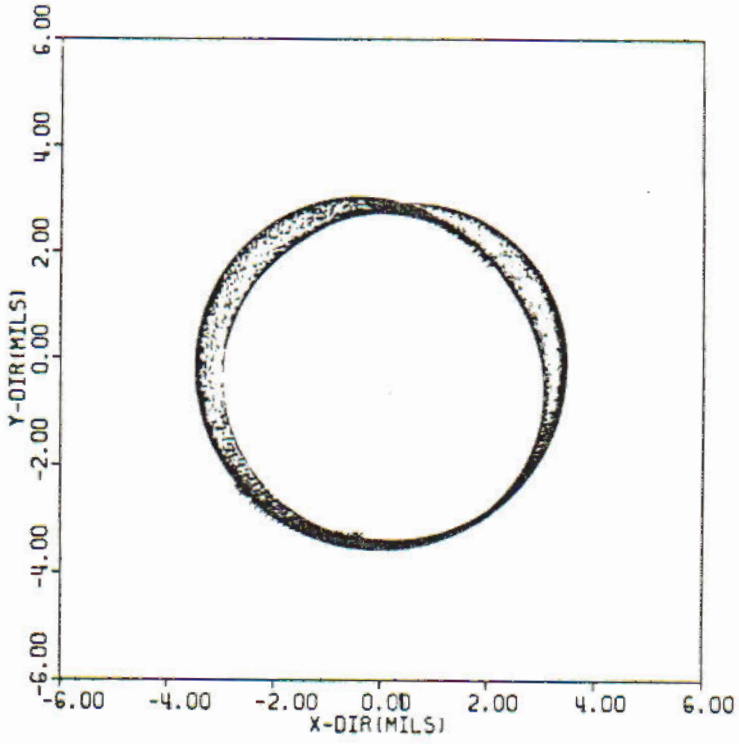

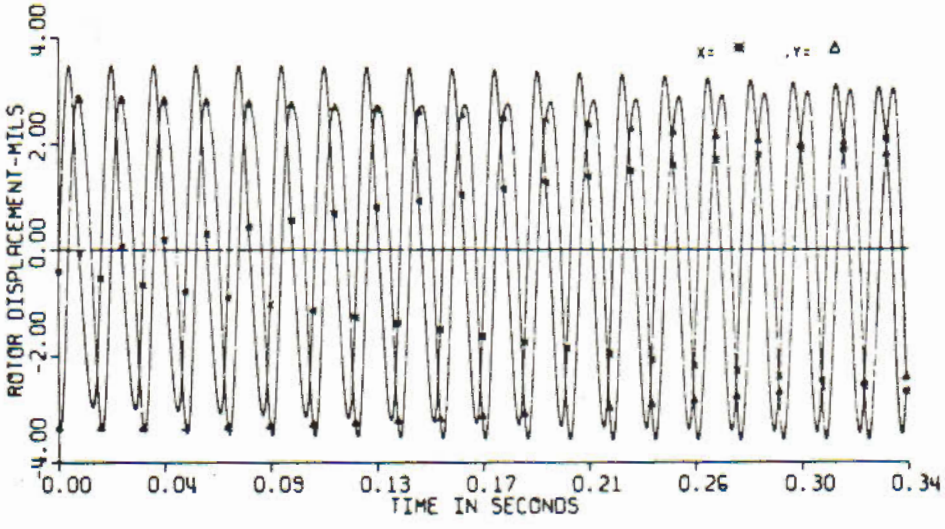

Fig. 12 Limit Cycle Simulation of 3-Mass Rotor with Fluid Film Bearings at 7,000 RPM

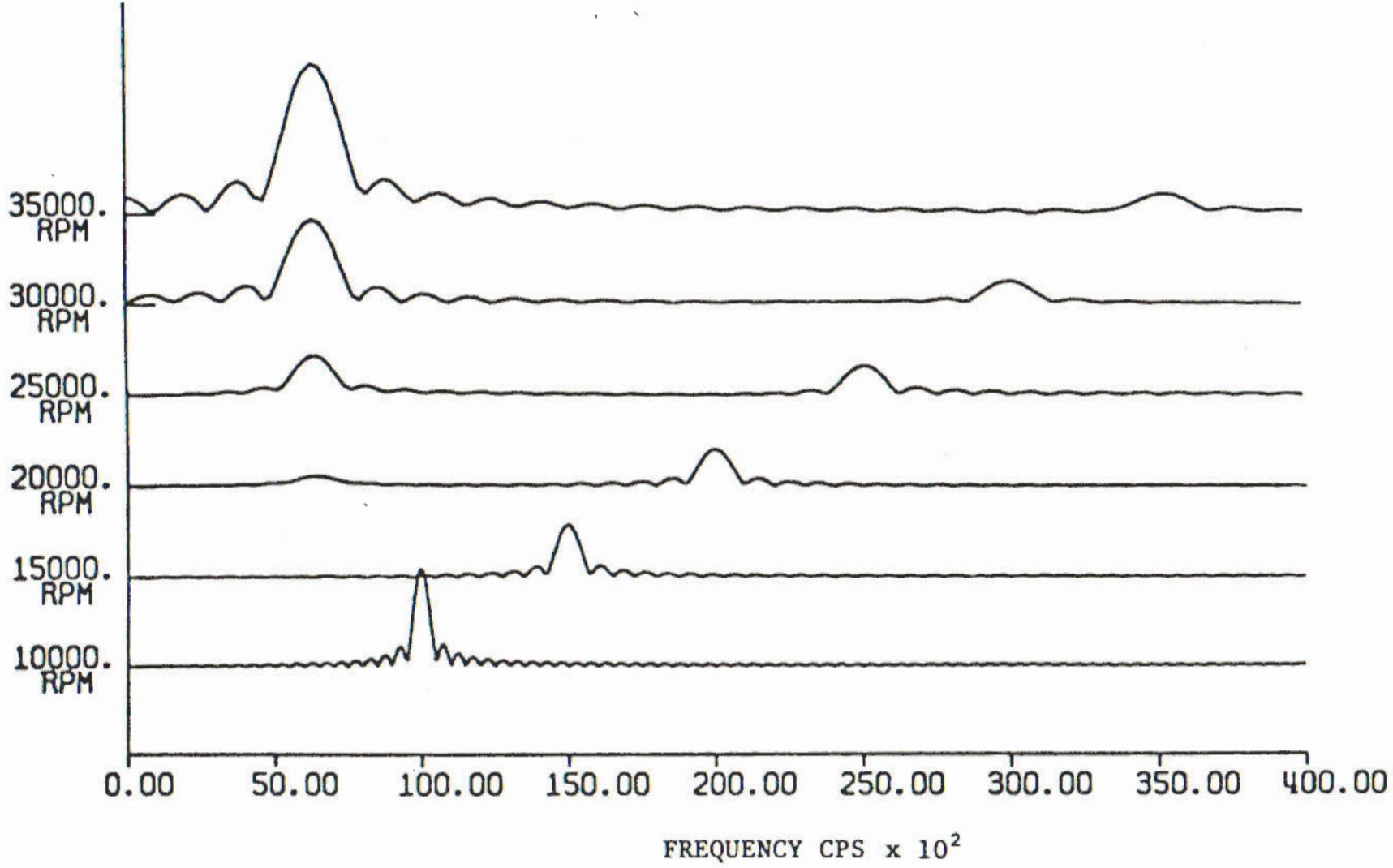

Fig. 13 Frequency Spectrum of 3-Mass Rotor with Fluid Film Bearings

The authors would also like to acknowledge the efforts of Mr. Malcolm Leader, Department of Mechanical and Aerospace Engineering, University of Virginia, for this development of the experimental data and to Bernard Herbage, President of Centritech Corporation, Houston, Texas, for the development of the experimental rotor facilities.

REFERENCES

1 Gunter, E. J. "Dynamic Stability of Rotor-Bearing Systems." NASA Report SP-113, 1965.

2 Lund, J. W. "Stability and Damped Critical Speeds of a Flexible Rotor in Fluid-Film Bearings." Journal of Engineering for Industry, Trans. ASME, May 1974, pp. 509-517.

3 Lund, J. W. and Orcutt, F. K. "Calculations and Experiments on the Unbalance Response of a Flexible Rotor." Journal of Engineering for Industry, Trans. ASME, Series B, Vol. 89, No. 4, November 1967, pp. 785-796.

4 Nicholas, J. C., Gunter, E. J., and Allaire, P. E. "Effect of Residual Shaft Bow on Unbalance Response and Balancing of a Single-Mass Rotor - Part 1: Unbalance Response." Journal of Engineering for Power, Trans. ASME, April 1976, pp. 171-181.

5 Black, H. F. and Nutall, S. M. "Modal Resolution and Balancing of Synchronous Vibrations in Flexible Rotors with Nonconservative Cross Coupling." Conference on Vibrations in Rotation Machinery, Instn. Mechanical Engineers, September 1976, pp. 151-158.

6 Nicholas, J. C., Gunter, E. J., and Allaire, P. E. "Effect of Residual Bow on Unbalance Response and Balancing of a Single-Mass Rotor - Part II: Balancing." Journal of Engineering for Power, Trans. ASME, April 1976, pp. 182-189.

7 Kirk, R. G., and E. J. Gunter. "Transient Response of Rotor-Bearing Systems." Journal of Engineering for Industry, Trans. ASME, May 1974.

8 Shen, F. A. "Transient Flexible Dynamic Analysis - Part 1: Theory." Journal of Engineering for Industry, May 1972.

9 Breed, D. and Castelli, V. "Time Transient Approach to the Solution of Shaft Dynamic Problems." Columbia University Ph.D. Dissertation, 1970.

10 Kirk, R. G., and Gunter, E. J. "Nonlinear Transient Analysis of Multi-mass Flexible Rotors." RLES Report No. ME-4040-112-72U, University of Virginia, June 1, 1972.

11 Foss, K. "Co-Ordinates Which Uncouple the Equations of Motion of Damped Linear Dynamic Systems." Journal of Applied Mechanics, Trans. ASME, September 1958.

12 Childs, D. W. "A Rotor-Fixed Modal Simulation Model for Flexible Rotating Equipment." Journal of Engineering for Industry, Trans. ASME, Series B, Vol. 96, No. 2, May 1974, pp. 659-669.

13 Childs, D. "A Modal Transient Simulation Model for Flexible Asymmetric Rotors." Journal of Engineering for Industry, Trans. ASME, Series B, Vol. 98, No. 1, February 1976, pp. 312-319.

14 Kirk, R. G., and Hibner, D. H. "A Note on Blade Loss Dynamics of Rotor-Bearing Systems," ASME Paper No. 75-DET-56.

15 Black, H. F. "Calculation of Forced Whirling and Stability of Centrifugal Pump Rotor Systems." Journal of Engineering for Industry, Trans. ASME, Paper No. 73-DET-131.

16 Lund, J. W. "Modal Response of a Flexible Rotor in Fluid Film Bearings." Journal of Engineering for Industry, Trans. ASME, May 1974.

17 Myrick, S. T., Jr., and Rylander, H. G. "Analysis of Flexible Rotor Whirl and Whip Using a Realistic Hydrodynamic Journal Bearing Model." Trans. ASME, Journal of Engineering for Industry, Paper No. 75-DET-68.

18 Choy, K. C. "Dynamic Analysis of Flexible Rotor-Bearing Systems Using Modal Approach." Ph.D. Thesis, University of Virginia, August 1977.

19 Gunter, E. J., Choy, K. C., and Allaire, P. E. "Modal Analysis of Turborotors Using Planar Modes - Theory." Accepted for Publication in Journal of the Franklin Institute, November 1977.

20 Leader, M. E., et al. "The Experimental Dynamic Response of a Single Mass Rotor in Three Different Bearings." Report No. UVA/464761/ME/76/141, December 1976, University of Virginia.

21 Lund, J. W. "Self-Excited, Stationary Whirl Orbits of a Journal in a Sleve Bearing." Ph.D. Thesis, Rensselaer Polytechnic Institute, 1966.

22 Kirk, R. and Gunter, E. J. "Transient Journal Bearing Analysis." NASA Report No. CR-154, June 1970.

23 Cooley, J. W., Lewis, P. A., and Welch, P. D. "Application of the Fast Fourier Transformation to Computation of Fourier Integrals, Fourier Series, and Convolution Integrals." IEEE Trans., Vol. AU-15, No. 2, June 1967.

24 Rabiner, L. R. and Rader, C. M. "Digital Signal Processing." IEEE Press, 1972.

APPENDIX A

General Equations of Motion

In deriving the general equations of motion for a multimass bearing system, the rotor is divided into discrete mass stations such that the dynamics of the rotor system can be represented by forces and displacements at the mass stations (18, 19). The rotor section between two consequentive mass stations is assumed to be massless while the weight of the rotor element is lumped at the two mass stations at each side of the element.

The system equations of motion can be written in matrix form as follows (18, 19):

$$[\bar{M}]\ \{\ddot{U}\} + [C]\ \{\dot{U}\} + [K]\ \{U\} = \{F(t)\} + [K_s]\ \{U_d\} \qquad (A.1)$$

The forcing function $\{F(t)\}$ due to shaft unbalance and disk skew is given by

$$\{F(t)\} = \begin{Bmatrix} F_x(t) \\ F_y(t) \\ M_x(t) \\ M_y(t) \end{Bmatrix}_i$$

where

$$\begin{Bmatrix} F_{xi}(t) \\ F_{yi}(t) \end{Bmatrix} = M_i e_i \left\{ \omega^2 \begin{bmatrix} \cos(\omega t + \alpha_i) \\ \sin(\omega t + \alpha_i) \end{bmatrix} + \dot{\omega} \begin{bmatrix} \sin(\omega t + \alpha_i) \\ -\cos(\omega t + \alpha_i) \end{bmatrix} \right\}$$

$$\begin{Bmatrix} M_{xi}(t) \\ M_{yi}(t) \end{Bmatrix} = \tau_i (I_p - I_t)_i \left\{ \omega^2 \begin{bmatrix} \cos(\omega t + \beta_i) \\ \sin(\omega t + \beta_i) \end{bmatrix} + \dot{\omega} \begin{bmatrix} \sin(\omega t + \beta_i) \\ -\cos(\omega t + \beta_i) \end{bmatrix} \right\}$$

also

$$U = \begin{Bmatrix} (x) \\ (\theta) \\ (y) \\ (\psi) \end{Bmatrix} \quad , \quad U_d = \begin{Bmatrix} (x_d) \\ (\theta_d) \\ (y_d) \\ (\psi_d) \end{Bmatrix}$$

and

$$[\bar{M}] = \begin{bmatrix} [M] & 0 & 0 & 0 \\ 0 & [I_t] & 0 & 0 \\ 0 & 0 & [M] & 0 \\ 0 & 0 & 0 & [I_t] \end{bmatrix}$$

The damping matrix can be decomposed into the gyroscopic and bearing damping submatrices for further convenience as follows:

$$[C] = \begin{bmatrix} 0 & 0 & 0 & 0 \\ 0 & 0 & 0 & [I_p] \\ 0 & 0 & 0 & 0 \\ 0 & [-I_p] & 0 & 0 \end{bmatrix}_G + \begin{bmatrix} [C_{xx}] & [C_{x\theta}] & [C_{xy}] & [C_{x\psi}] \\ [C_{\theta x}] & [C_{\theta\theta}] & [C_{\theta y}] & [C_{\theta\psi}] \\ [C_{yx}] & [C_{y\theta}] & [C_{yy}] & [C_{y\psi}] \\ [C_{\psi x}] & [C_{\psi\theta}] & [C_{\psi y}] & [C_{\psi\psi}] \end{bmatrix}$$

The general stiffness matrix may also be decomposed into three submatrices representing the symmetric shaft stiffness matrix, the linear bearing stiffness matrix, and the skew symmetric acceleration matrix as follows

$$[K] = \begin{bmatrix} [k_{xx}] & [k_{x\theta}] & 0 & 0 \\ [k_{\theta x}] & [k_{\theta\theta}] & 0 & 0 \\ 0 & 0 & [k_{xx}] & [k_{x\theta}] \\ 0 & 0 & [k_{\theta x}] & [k_{\theta\theta}] \end{bmatrix}_S + \begin{bmatrix} [K_{xx}] & [K_{x\theta}] & [K_{xy}] & [K_{x\psi}] \\ [K_{\theta x}] & [K_{\theta\theta}] & [K_{\theta y}] & [K_{\theta\psi}] \\ [K_{yx}] & [K_{y\theta}] & [K_{yy}] & [K_{y\psi}] \\ [K_{\psi x}] & [K_{\psi\theta}] & [K_{\psi y}] & [K_{\psi\psi}] \end{bmatrix}_B$$

$$+ \begin{bmatrix} 0 & 0 & 0 & 0 \\ 0 & 0 & 0 & \left[\frac{\dot{\omega}}{2} I_p\right] \\ 0 & 0 & 0 & 0 \\ 0 & \left[-\frac{\dot{\omega}}{2} I_p\right] & 0 & 0 \end{bmatrix}_A \qquad (A.3)$$

For free-free boundary conditions, the shaft stiffness submatrices are given by

$$[k_{xx}] = 2 \begin{bmatrix} E_1 & -E_1 & 0 & \cdots & 0 & 0 \\ -E_1 & E_1+E_2 & -E_2 & \cdots & 0 & 0 \\ \cdots & \cdots & \cdots & -E_{n-2} & E_{n-2}+E_{n-1} & -E_{n-1} \\ 0 & 0 & 0 & 0 & -E_{n-1} & E_{n-1} \end{bmatrix}$$

$$[k_{x\theta}] = [k_{\theta x}]^T =$$

$$\begin{bmatrix} E_1 L_1 & E_1 L_1 & 0 & \cdots & 0 & 0 \\ -E_1 L_1 & -E_1 L_1 + E_2 L_2 & E_2 L_2 & \cdots & 0 & 0 \\ \cdots & \cdots & \cdots & -E_{n-2} L_{n-2} & -E_{n-2} L_{n-2} + E_{n-1} L_{n-1} & E_{n-1} L_{n-1} \\ 0 & 0 & \cdots & 0 & -E_{n-1} L_{n-1} & -E_{n-1} L_{n-1} \end{bmatrix}$$

$$[k_{\theta\theta}] =$$

$$\frac{1}{3}\begin{bmatrix} 2E_1L_1^2 & E_1L_1^2 & 0 & 0 & 0 & 0 \\ E_1L_1^2 & 2E_1L_1^2+2E_2L_2^2 & E_2L_2^2 & 0 & 0 & 0 \\ \cdots\cdots & \cdots\cdots\cdots & \cdots & E_{n-2}L_{n-2}^2 & 2E_{n-2}L_{n-2}^2+2E_{n-1}L_{n-1}^2 & E_{n-1}L_{n-1}^2 \\ 0 & 0 & \cdots & 0 & 0 & 2E_{n-1}L_{n-1}^2 \end{bmatrix}$$

where $E_i = \left(\frac{6EI}{L^3}\right)_i$

APPENDIX B

Nonlinear Fluid Film Forces

This appendix develops the nonlinear fluid film forces for a short journal bearing. The analytical expressions are then directly employed in the modal transient equations. The Reynolds equation for short journal bearings in nondimensional form can be written as (20)

$$\frac{\partial}{\partial\xi}\left(h^3\frac{\partial P}{\partial\xi}\right) = (1 - 2\dot{\phi})\frac{\partial h}{\partial\theta} + 2\dot{\varepsilon}\cos\Omega \qquad (B.1)$$

where $P = \dfrac{\bar{P}}{6\mu\omega\left(\frac{R}{C}\right)^2}$

$h = \dfrac{\bar{h}}{C} = 1 + \varepsilon\cos\Omega$, $\dot{\phi}/\omega$

$\xi = \dfrac{z}{R}$

Using the boundary conditions of pressure $P = 0$ at $\xi = 0$ and $\xi = 1$, we have

$$P = \frac{1}{2}\left[\left(\frac{L}{D}\right)^2 - \xi^2\right]\frac{1}{h^3}\left[\varepsilon(1 - 2\dot{\phi})\sin\Omega - 2\dot{\varepsilon}\cos\Omega\right] \qquad (B.2)$$

Integrating the pressure using the half Sommerfeld condition as given by Lund (21), the bearing forces are calculated to be

$$f_r = \varepsilon(1 - 2\dot{\phi})\left(-2\int_{\Omega_1}^{\Omega_2}\frac{\cos\Omega\sin\Omega}{h^3}\,d\Omega\right) + 2\dot{\varepsilon}\left(2\int_{\Omega_1}^{\Omega_2}\frac{\cos^2\Omega}{h^3}\,d\Omega\right) \qquad (B.3)$$

$$f_t = \varepsilon(1 - 2\dot{\phi})\left(2\int_{\Omega_1}^{\Omega_2}\frac{\sin^2\Omega}{h^3}\,d\Omega\right) + 2\dot{\varepsilon}\left(-2\int_{\Omega_1}^{\Omega_2}\frac{\cos\Omega\sin\Omega}{h^3}\,d\Omega\right) \qquad (B.4)$$

where $\frac{F}{W} = \sigma f \quad , \quad \sigma = \frac{1}{8}\frac{\mu_0 DL}{W}\left(\frac{L}{C}\right)^2$

The integral can be evaluated as

$$-2\int_{\Omega_1}^{\Omega_2} \frac{\cos\Omega \sin\Omega}{h^3}\, d\Omega = \pm 4\, \frac{\varepsilon \cos^3\Omega_0}{[1 - \varepsilon^2 \cos^2\Omega_0]^2} \begin{cases} + \text{ for } (1 - 2\dot{\phi}) > 0 \\ - \text{ for } (1 - 2\dot{\phi}) < 0 \end{cases}$$

$$2\int_{\Omega_1}^{\Omega_2} \frac{\cos^2\Omega}{h^3}\, d\Omega = \frac{\pi(1 + 2\varepsilon^2)}{(1 - \varepsilon^2)^{5/2}} \pm \left\{ \frac{2(1 + 2\varepsilon^2)}{(1 - \varepsilon^2)^{5/2}} \tan^{-1}\alpha \right.$$

$$\left. - \frac{u}{(1 - \varepsilon^2)^2} \left[\frac{(3 - 5a^2)\, u^2 + (5 - 3a^2)\, a^2}{(u^2 + a^2)^2} + \frac{(3 - 5a^2) + (5 - 3a^2)\, a^2 u^2}{(1 + a^2 u^2)^2} \right] \right\}$$

and

$$2\int_{\Omega_1}^{\Omega_2} \frac{\sin^2\Omega}{h^3}\, d\Omega = \frac{2}{(1 - \varepsilon^2)^{3/2}} \left\{ \frac{\pi}{2} \pm \left[\tan^{-1}\alpha - \frac{a\, u(u^2 - a^2)}{(u^2 + a^2)^2} \right.\right.$$

$$\left.\left. - \frac{a\, u(1 - a^2 u^2)}{(1 + a^2 u^2)^2} \right] \right\} \begin{pmatrix} + \text{ for } \dot{\varepsilon} > 0 \\ - \text{ for } \dot{\varepsilon} < 0 \end{pmatrix}$$

where

$$u = \sqrt{\frac{1 - \cos\Omega}{1 + \cos\Omega}} \quad , \quad \cos\Omega_0 = \frac{\varepsilon\,|1 - 2\dot{\phi}|}{\sqrt{\varepsilon^2(1 - 2\dot{\phi})^2 + (2\dot{\varepsilon})^2}}$$

$$a^2 = \frac{1 + \varepsilon}{1 - \varepsilon}$$

$$\alpha = \left(\frac{u}{a}\right)\left(\frac{a^2 - 1}{1 + u^2}\right)$$

The bearing forces can be transformed into fixed x, y coordinates by

$$F_x = \left[-(f_r\, x + f_t\, y)/\sqrt{x^2 + y^2} \right]\sigma$$

$$F_y = \left[(-f_r\, y + f_t\, x)/\sqrt{x^2 + y^2} \right]\sigma$$